

---

**SPECIAL ISSUE ARTICLE****Field of the paper**

# Evidence for Phenotype-Driven Disparities in Freezing of Gait Detection and Approaches to Bias Mitigation

Timothy Odonga<sup>1</sup> | Christine D. Esper<sup>1</sup> | Stewart A. Factor<sup>1</sup> | J. Lucas McKay<sup>†1,2</sup> | Hyeokhyen Kwon<sup>†1,2</sup>

<sup>1</sup>Emory University

<sup>2</sup>Georgia Institute of Technology

**Correspondence**

Department of Biomedical Informatics,  
Emory University, Atlanta, GA, USA  
Email: lucas@dbmi.emory.edu;  
hyeokhyen.kwon@dbmi.emory.edu

**Present address**

Department of Biomedical Informatics,  
Emory University, Atlanta, Georgia, USA

†These authors contributed equally to this work as senior authors.

**Funding information**

Freezing of gait (FOG) is a debilitating feature of Parkinson's disease (PD) and a common cause of injurious falls. Recent advances in wearable-based human activity recognition (HAR) have enabled FOG detection, but bias and fairness in these models remain understudied. Bias is defined as a systematic error that leads to unequal outcomes, while fairness refers to consistent performance across subject groups. Biased models could systematically underserve patients with specific FOG phenotypes or demographics, potentially widening care disparities. We systematically evaluated the bias and fairness of state-of-the-art HAR models for FOG detection across FOG phenotypes and patient demographics using multi-site datasets. Four mitigation approaches were assessed, including conventional bias mitigation approaches (threshold optimization and adversarial debiasing) and two transfer learning-based approaches (multi-site transfer and fine-tuning large pretrained models). Fairness was primarily quantified using the demographic parity ratio (DPR) and the equalized odds ratio (EOR). HAR models exhibited substantial bias (DPR & EOR  $< 0.8$ ) across all variables, including age, sex, disease duration, and critically, FOG phenotype.

---

**Abbreviations:** FOG, freezing of gait; PD, Parkinson's disease; HAR, human activity recognition; ML, machine learning.

This phenotype-specific bias is particularly concerning as tremulous and akinetic FOG may require different clinical management. Conventional bias mitigation methods failed: threshold optimization ( $DPR=-0.126$ ,  $EUR=+0.063$ ) and adversarial debiasing ( $DPR=-0.008$ ,  $EUR=-0.001$ ). In contrast, transfer learning from multi-site datasets significantly improved fairness ( $DPR=+0.037$ ,  $p<0.01$ ;  $EUR=+0.045$ ,  $p<0.01$ ) and performance ( $F1\text{-score}=+0.020$ ,  $p<0.05$ ). Transfer learning across diverse datasets is essential for developing equitable HAR models that reliably detect FOG across all patient phenotypes, ensuring wearable-based monitoring benefits all individuals with PD. **Keywords** — Parkinson's Disease, Wearable Sensors, Human Activity Recognition

## 1 | INTRODUCTION

Freezing of gait (FOG) is a debilitating symptom of Parkinson's disease (PD) that is challenging for clinicians to capture and evaluate during time-limited clinical assessments (Nutt et al., 2011). This is primarily due to the brief, sudden, and episodic nature of FOG, which makes it challenging to assess on demand (Nutt et al., 2011; Gilat et al., 2026). Furthermore, clinical assessments may not fully capture FOG as subjects' gait typically improves when focusing on walking during evaluation (Hallett, 2008), typically well-lit hospital environments limit the occurrence of FOG as subjects use visual feedback to compensate for gait (Barthel et al., 2016), and subjects often are evaluated when in an on-medication state that has less occurrence of FOG in comparison to the off-medication state (Schaafsma et al., 2003; McKay et al., 2019). Consequently, there is a need to assess FOG beyond routine clinical visits to facilitate more accurate clinician assessment (Mancini et al., 2019).

Machine learning approaches using wearable or kinematic data show promise for objectively detecting FOG and enabling automated assessment (Kwon et al., 2023; Filtjens et al., 2022; Mancini et al., 2025; Salomon et al., 2024; Yang et al., 2024). Studies have shown that wearable sensors can provide objective FOG assessment with sensitivity and specificity values exceeding 90% across different sensor configurations, provoking tasks, detection algorithms, and validation settings (Reches et al., 2020; Pardoel et al., 2019). Recent studies have also shown that kinematic marker data from optical motion capture systems enable automated FOG assessment, with deep learning approaches achieving expert-level performance and identifying features consistent with expert assessments (Filtjens et al., 2022; Kwon et al., 2023).

One complicating feature of FOG is that it manifests in distinct phenotypes, such as tremulous and akinetic forms, which may reflect different underlying pathophysiology and treatment needs (Factor et al., 2025). Akinetic FOG involves impairments across motor, cognitive, and limbic basal ganglia circuits and emerges predominantly during gait initiation and dual-tasking, while tremulous FOG reflects relatively preserved cognitive and limbic function with unsuccessful stepping attempts that predominate during turning (Koehler et al., 2021; Zoetewei et al., 2025). Emerging research further suggests that FOG may develop through dysfunctional feedback loops involving norepinephrine depletion, neuroinflammation, and amyloid- $\beta$  accumulation beyond primary dopaminergic pathology (Factor et al.,

2025). Phenotype-specific detection challenges may thus contribute to systematic differences in automated FOG assessment.

Few of these models have been comprehensively evaluated for performance across phenotypes, which could potentially introduce systematic error. Best practices for evaluating differential performance have yet to be established. Few prior studies have reported phenotype-stratified performance; limited evidence available from one study (Yang et al., 2024) suggests higher performance for tremulous compared with akinetic FOG (intraclass correlation coefficient [ICC] roughly 0.86 vs. 0.78). However, this work focused on optimizing detection accuracy rather than systematically assessing differential performance across phenotypes. Performance was not examined across subject groups, nor were potential contributors to reduced accuracy in akinetic FOG explored. Given that tremulous and akinetic manifestations co-occur in over 80% of patients (Zoetewei et al., 2025), systematic evaluation of performance differences across FOG manifestations remains an important gap.

At the same time, the machine learning community has established methods to quantify bias, as well as fairness approaches to mitigate bias in such models. Bias is defined as systematic errors leading to unequal outcomes (Ferrara, 2023), while fairness is defined as consistent performance across subject groups (Varshney, 2022). Bias can be quantified across subject groups at different levels of analysis, including metrics based solely on predicted outcomes and metrics that compare predicted outcomes against actual labels (Verma and Rubin, 2018). Bias mitigation approaches operate at different stages of the modeling pipeline: pre-processing methods address imbalanced training data, in-processing methods incorporate fairness constraints into model optimization (Zhang et al., 2018), and post-processing methods adjust decision thresholds to equalize performance across groups (Hardt et al., 2016). Such techniques have been successfully applied to reduce disparities in applications such as clinical risk prediction and diagnostic imaging algorithms (Sivarajkumar et al., 2023; Yang et al., 2023; Siddiqui et al., 2024). However, these established fairness methods have not been systematically applied to FOG detection models, leaving it unclear whether they can effectively mitigate differential performance across FOG manifestations.

To the best of our knowledge, no prior work has applied the frameworks of fairness in machine learning (Fair ML) to investigate bias and fairness in wearable-based FOG detection, despite its critical importance for developing unbiased models capable of measuring FOG accurately across phenotypes or demographic strata. While a few studies in FOG and PD research have reported performance differences across subject subgroups, these analyses were limited to post hoc statistical comparisons and did not employ fair machine learning techniques to address the identified differences. In FOG detection, Kwon et al. (2023) computed individual-level F1 scores for each participant and compared performance across age, sex, and study groups using linear regression with Wald tests for statistical significance. In broader PD digital biomarker research, Zhang et al. (2020) performed stratified analyses by calculating performance metrics with 95% confidence intervals for each demographic stratum and conducting pairwise bootstrap comparisons, while Khera and Kumar (2022) trained separate prediction models for different age-gender groups and compared classification accuracies using 10-fold cross-validation. Adnan et al. (2025) reported performance differences across sex and ethnic subject groups for PD screening from facial videos. However, neither study quantified bias using Fair ML metrics or applied bias mitigation strategies, and wearable-based FOG detection remains entirely unexamined across phenotypic and demographic subject groups.

To address this gap, we implemented five existing state-of-the-art human activity recognition (HAR) models (Breiman, 2001; Ordóñez and Roggen, 2016; Haresamudram et al., 2020; Yuan et al., 2024; Ruan et al., 2025) for FOG detection and systematically evaluated their bias and fairness across FOG phenotypes and demographic strata. We used four multi-site datasets to make our approach as representative as possible (Roggen et al., 2013; Ribeiro De Souza et al., 2022; Howard et al., 2023). Models were implemented either by deploying open-source code from original publications or by replicating published architectures. We used three common notions of group fairness to comprehensively

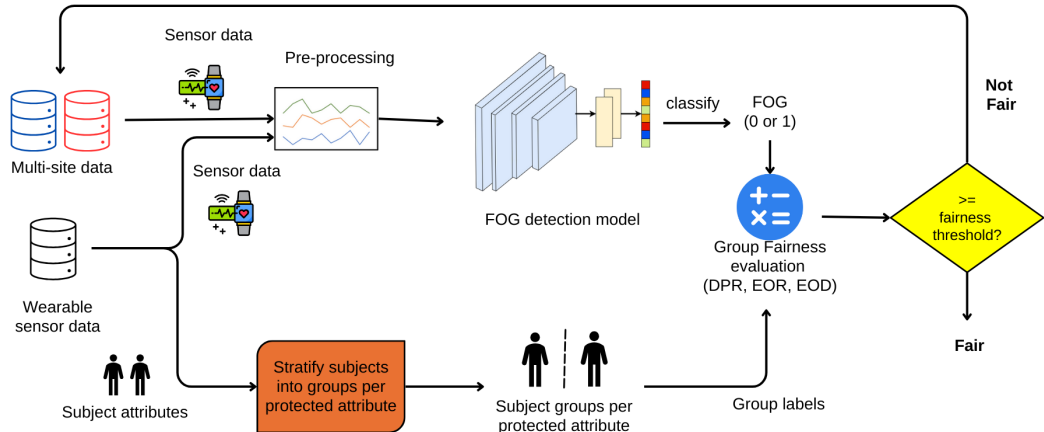


**FIGURE 1** Model bias evaluation pipeline for FOG detection tasks. In this work, we analyze the group fairness of the model based on protected attributes in FOG and PD, including FOG phenotype, sex, age, and disease duration.

evaluate the FOG detection models (Verma and Rubin, 2018). Demographic parity assesses whether positive prediction rates are equal across subject groups (Dwork et al., 2012). Equalized odds require equal true positive and false positive rates across subject groups conditional on the true outcome (Hardt et al., 2016). Equal opportunity, a relaxation of equalized odds, requires only equal true positive rates across subject groups (Hardt et al., 2016). These three notions offered complementary perspectives on fairness, assessing both prediction patterns and prediction accuracy across subject groups (Verma and Rubin, 2018). Lastly, we implemented various bias mitigation approaches, such as threshold optimization (Hardt et al., 2016) and adversarial debiasing (Zhang et al., 2018), as well as transfer learning-based approaches using multi-site data and large-scale pretrained models to assess the extent to which these approaches would mitigate biases.

Our findings demonstrated that approaches from Fair ML can evaluate and potentially improve FOG model performance across phenotypes, subject demographics, or other variables. Fair ML approaches combined with stratified sampling during data collection could help ensure model performance reflects behavior across all groups rather than appearing strong overall while performing poorly for specific groups (Mitani et al., 2021; Mehrabi et al., 2021). Ultimately, addressing fairness in FOG detection is essential for realizing the promise of wearable-based monitoring for objective assessment of FOG across phenotypes and demographics.

## 2 | METHODS

### 2.1 | Overall Approach

Here, we describe the definitions and metrics of bias and fairness used in our analysis, the four multi-site datasets, the HAR models implemented, the bias mitigation approaches, and the experimental settings used to evaluate FOG detection performance and model biases in this work. Figure 1 shows the overall framework of our evaluation.

## 2.2 | Definitions of Bias and Fairness

In this section, we define protected attributes, bias, and fairness. We then describe the notions of group fairness evaluated in this study and the metrics used to quantify them.

Protected attributes are attributes of an individual that may not be used directly or indirectly as a basis for automated decision-making in order to prevent systematic advantage accorded to specific groups in automated decision-making processes (Dwork et al., 2012; Varshney, 2022). While no fixed set of protected attributes exists, this work considers clinical attributes, such as FOG phenotype and disease duration, as well as demographic characteristics, such as age and sex. Model performance should be consistent across groups defined by these attributes, ensuring that model predictions are independent of these attributes (Dwork et al., 2012; Varshney, 2022).

Bias in automated decision support systems is defined as systematic errors leading to unequal outcomes (Ferrara, 2023). Fairness can be defined at the individual level (similar treatment for similar individuals) or at the group level (equal behavior across demographic groups) (Dwork et al., 2012; Varshney, 2022). This work adopts a group fairness definition, whereby fairness is satisfied when average model performance is consistent across groups defined by protected attributes (e.g., FOG phenotype, age, sex) (Varshney, 2022).

Demographic parity requires equal proportions of positive predictions between protected groups (e.g., equal rate of detected FOG episodes from the model) (Dwork et al., 2012). In this work, demographic parity was computed using the **Demographic Parity Ratio (DPR)** defined below (Weerts et al., 2023).

$$DPR = \frac{P(F_{pred} = 1|G = g_i)}{P(F_{pred} = 1|G = g_j)} \quad (1)$$

where  $F_{pred}$  is the model's detection of an FOG episode,  $i \neq j$ ,  $g_i$  and  $g_j$  are binary groups derived from a protected attribute G and  $P(F_{pred} = 1|G = g_i) \leq P(F_{pred} = 1|G = g_j)$ .

Equality of opportunity (true positive parity) is satisfied when protected groups benefit equally from correct model predictions (e.g., a model correctly detects an FOG episode) (Hardt et al., 2016). Conversely, false positive parity requires equal rates of incorrect positive predictions across groups (e.g., a model detects a false FOG episode) (Hardt et al., 2016). True positive parity ratio (TPPR) and false positive parity ratio (FPRR) are defined as shown below (Hardt et al., 2016).

$$TPPR = \frac{P(F_{pred} = 1|F_{true} = 1, G = g_i)}{P(F_{pred} = 1|F_{true} = 1, G = g_j)}$$

$$FPRR = \frac{P(F_{pred} = 1|F_{true} = 0, G = g_i)}{P(F_{pred} = 1|F_{true} = 0, G = g_j)}$$

where  $F_{pred}$  is the model's output,  $F_{true}$  is the ground truth annotation for an FOG episode,  $i \neq j$ ,  $g_i$  and  $g_j$  are binary groups derived from a protected attribute G and  $P(F_{pred} = 1|G = g_i) \leq P(F_{pred} = 1|G = g_j)$ . Equality of opportunity was computed using the **Equality of Opportunity Difference (EOD)** (Weerts et al., 2023):

$$EOD = P(F_{pred} = 1|F_{true} = 1, G = g_i) - P(F_{pred} = 1|F_{true} = 1, G = g_j) \quad (2)$$

Equalized odds are satisfied when the true positive parity and the false positive parity are equal across groups (Hardt et al., 2016). Equalized odds were computed using the **Equalized Odds Ratio (EOR)**, which captures the worst-case

**TABLE 1** Characteristics of datasets used in this study. Numerical values are presented as mean  $\pm$  standard deviation. N denotes the number of subjects, M refers to male, and F refers to female.

Dataset	N	Sex	Age (years)	Disease Duration (years)	Frequency (Hz)	Sensor locations	Label distribution	FOG type distribution	Average recording length per subject (minutes)	Total dataset recording length (hours)
Daphnet	10	M=7 F=3	66 $\pm$ 5	13.7 $\pm$ 9.7	64	Ankle, Lower back, Thigh	No FOG=0.90 FOG=0.10	Tremulous=0.95 Akinetic=0.05	29.6 $\pm$ 6.8	4.9
De Souza	35	M=19 F=16	65 $\pm$ 10	8.0 $\pm$ 4.1	128	Shank	No FOG=0.80 FOG= 0.20	Tremulous=0.97 Akinetic=0.03	4.1 $\pm$ 1.7	2.4
DeFOG	38	M=24 F=14	67 $\pm$ 9	9.5 $\pm$ 5.5	100	Lower back	No FOG=0.95 FOG=0.05	Tremulous=0.63 Akinetic=0.37	59.3 $\pm$ 31.7	15.0
tDCS FOG	62	M=50 F=12	69 $\pm$ 8	12.4 $\pm$ 6.7	128	Lower back	No FOG=0.68 FOG=0.32	Tremulous=0.86 Akinetic=0.14	14.5 $\pm$ 16.8	37.5

disparity between groups, as shown below (Hardt et al., 2016; Weerts et al., 2023).

$$EOR = \min(TPPR, FPRR) \quad (3)$$

## 2.3 | Wearable Datasets for FOG

To effectively evaluate FOG detection performance across phenotypic and demographic groups, four publicly available multi-site FOG datasets were selected based on variation in sensor locations, FOG-provoking protocols, and the location of clinical assessment (i.e., clinic versus home). Across datasets, there were a total of N=145 individuals with PD, of whom 31% were women, the average age was  $67 \pm 9$  years, and the average disease duration was  $10 \pm 6$  years. All of the datasets used common inertial measurement unit (IMU) instrumentation with varied sensor locations across the lower back, ankle, shank, and thigh. All of them exhibited a significant label imbalance with No FOG predominating the recorded samples (86% on average) and tremulous FOG much more prevalent than akinetic FOG (82% on average). Importantly, these datasets contain sample-level FOG annotations enabling extraction and phenotypic classification of individual FOG episodes (Moore et al., 2013). The specifics of the FOG-provoking protocols varied substantially across datasets, including Timed Up & Go (Podsiadlo and Richardson, 1991), Hotspot Door tasks (Howard et al., 2023), motor cognitive tasks (Reches et al., 2020), daily walking tasks (Bächlin et al., 2010), and turning tasks (Ribeiro De Souza et al., 2022). These details are summarized in Table 7. Characteristics of each included dataset are summarized in Table 1.

## 2.4 | Pipeline and HAR Models

To effectively capture FOG episodes and examine bias in the state-of-the-art HAR models, we first processed our data using established activity recognition approaches, including the sliding window approach (Bulling et al., 2014). Reported optimal window sizes that maximized FOG detection performance were used to segment recordings into non-overlapping windows for FOG detection, namely, 3-second windows for tDCSFOG, DeFOG, and DeSouza (Reches et al., 2020), and a 4.5-second window for Daphnet (Bächlin et al., 2010). Additionally, Min-Max scaling was applied to each sensor channel across all subject readings to accelerate model convergence during training (Rosati et al., 2018).

We selected five HAR model types to represent the current state of the art while maintaining an element of parsimony. (Breiman, 2001; Ordóñez and Roggen, 2016; Haresamudram et al., 2020; Yuan et al., 2024; Ruan et al., 2025). The first three HAR models (referred to as **Models A1-A3**) represent well-established HAR methodologies commonly available in the literature and were trained from scratch: Random Forest (RF; **Model A1**), a deep convo-

lutional and long short-term memory model (DeepConvLSTM; **Model A2**) (Ordóñez and Roggen, 2016), and Masked Transformer (**Model A3**) (Haresamudram et al., 2020). These models represent a class of architectures commonly used for tasks such as detecting daily activities (e.g., walking, sitting, standing), detecting sports and exercise movements, and gesture recognition (Zappi et al., 2008; Roggen et al., 2010).

Model A1 and A2 were selected based on their known ability to classify complex activities in daily living and locomotion (Kwon et al., 2019). Model A3 was selected because of the ability of transformer-based models to model long-range dependencies and sequence data (Vaswani et al., 2017). For Model A1, we extracted features from each analysis window using the empirical distribution function (ECDF) to obtain nonparametric, length-invariant representations that preserve the empirical distributions of each sensor channel (Hammerla et al., 2013). Following Ordóñez and Roggen (Ordóñez and Roggen, 2016), the raw sensor time series were provided to the deep learning-based models (Models A2-A3). To enable real-time prediction of the onset or offset of FOG episodes during subject movement, each analysis window was labeled as having an FOG episode or normal movement based on the annotation at the last timestep of the window (Yao et al., 2018).

We also fine-tuned two large-scale pretrained models (also referred to as foundation models) (**Models B1-B2**): a HAR-based pretrained model (Yuan et al., 2024) (**Model B1**) and a foundation model based on actigraphy data (Ruan et al., 2025) (**Model B2**). In general, these models offer improved recognition in use cases like activity classification, sleep abnormality detection, and mental health biomarker detection (Yuan et al., 2024; Ruan et al., 2025). They differ from models A1-A3 in that they are pretrained on petabyte-scale data that may provide useful "inherited" features learned during pretraining, potentially improving performance on downstream classification tasks even with limited labeled training data. Model B1 is a residual network-based (ResNet) convolutional model pretrained on general human activities (e.g., walking, sitting, cycling) from UK Biobank (Yuan et al., 2024), while Model B2 is a transformer-based model pretrained on actigraphy data (Ruan et al., 2025). While ResNet's convolutional layers excel at detecting local patterns but struggle with long-range dependencies, transformers can capture relationships across distant time points through their attention mechanisms (He et al., 2016; Vaswani et al., 2017). Similar to Model A2-A3, the raw sensor time series were provided to Models B1-B2 (Ordóñez and Roggen, 2016).

## 2.5 | Bias Mitigation

We implemented four bias mitigation approaches spanning the full machine learning pipeline and compared established fairness methods with novel transfer learning approaches to identify which strategies most effectively reduced bias in FOG detection models. Two established methods (threshold optimization and adversarial debiasing) have demonstrated effectiveness in fairness applications across other domains such as finance (Hardt et al., 2016; Zhang et al., 2018). We additionally evaluated two transfer learning approaches (leveraging multi-site data and pretrained models) that we hypothesized would improve fairness by exposing models to more diverse training examples. Due to architectural constraints and practical considerations, we applied each mitigation approach only to models for which prior literature suggested optimal performance and technical feasibility. For example, adversarial debiasing requires gradient-based optimization and therefore could not be applied to Model A1 (Random Forest) (Zhang et al., 2018). Similarly, threshold optimization was not applied to the deep learning models (Models A2-A3), as it has been shown to be suboptimal for correcting biases encoded in deep learning models' learned representations (Chen et al., 2023; Kpatcha, 2025).

Threshold optimization, known for its effectiveness with shallow models, was applied to Model A1 to reduce bias quantified by DPR, EOR, and EOD between the protected groups (Hardt et al., 2016). The concept of threshold optimization is a post-processing bias mitigation method that adjusts decision thresholds derived from a model's

score distribution, separately for different protected groups, to reduce differences in error or selection rates without retraining the model (Hardt et al., 2016). Similar to using sensitivity or specificity to identify an optimal operating point for a generic classifier, threshold optimization selects group-specific thresholds that satisfy fairness criteria, enabling a controlled trade-off between accuracy and group fairness (Hardt et al., 2016). Decision thresholds for each protected group were adjusted to satisfy demographic parity, true positive parity, and equalized odds in our implementation (Hardt et al., 2016). To mimic real-world deployment scenarios, threshold optimization was applied only to the train and validation splits to calibrate the decision thresholds, with evaluation conducted on the test data (Weerts et al., 2023; Hardt et al., 2016).

We applied adversarial debiasing to train attribute-agnostic feature representations in the implemented FOG detection models (Zhang et al., 2018). The concept of adversarial debiasing is that two competing neural networks are trained simultaneously: the main classifier learns to detect FOG episodes while a second "adversarial" model examines the main classifier's internal representations and attempts to identify protected attributes (such as age or sex) from them (Zhang et al., 2018). During training, the main classifier receives a penalty whenever the adversarial model successfully identifies these attributes, forcing it to learn patterns (in this case, FOG patterns) that do not encode demographic or clinical characteristics (Zhang et al., 2018). By combining the main model's performance with the penalty from the adversarial model, this approach aims to create a classifier that performs FOG detection without relying on protected attributes. This was implemented with two simultaneously trained neural networks: our deep-learning predictor model (Model A2 or A3) and a two-layer multi-layer perceptron (MLP) serving as the adversary (Zhang et al., 2018; Weerts et al., 2023). The predictor model was trained to accurately detect FOG episodes while the adversary network tried to predict the protected attribute from the predictor's learned representations (Zhang et al., 2018). To learn attribute-agnostic features, the training minimizes the loss defined as  $\nabla_W L_P - \text{proj}_{\nabla_W L_A} \nabla_W L_P - \alpha \nabla_W L_A$ , where  $L_P$  is the classification loss for the predictor model,  $L_A$  is the adversary loss for the adversary model, and  $\alpha$  is a hyperparameter that controls the strength with which the fairness constraint is enforced (Zhang et al., 2018). We experimented with two approaches: single attribute debiasing (training separate adversaries for each protected attribute) and a multi-head debiasing approach that implemented the adversary as a multi-head MLP to debias the protected attributes (FOG phenotype, age, sex, and disease duration) concurrently (Zhang et al., 2018). We hypothesized that multi-head adversarial debiasing would yield a fairer model across all attributes by simultaneously modeling their interplay.

To address dataset homogeneity, we experimented with transfer learning across multi-site FOG datasets. We hypothesized that diversifying training data would simultaneously improve fairness and model performance. To the best of our knowledge, this represents the first application of transfer learning for bias mitigation in FOG detection. Since the datasets contained readings from different sensor locations (e.g., lower back, ankle), transfer learning required matching both sensor placements and sampling frequencies between the source and target datasets (Chakma et al., 2021; Link et al., 2022). Sensor locations were paired to ensure comparable on-body locations: lower extremity sensors (ankle, thigh, shank) for Daphnet and De Souza transfers, and lower-back sensors for multi-source combinations involving DeFOG (DeFOG + Daphnet  $\rightarrow$  tDCS FOG; tDCS FOG + Daphnet  $\rightarrow$  DeFOG). Sampling frequencies were harmonized by downsampling all datasets to the lowest frequency in each pairing (e.g., 64 Hz when Daphnet was included). For Model A2-A3, the first two convolutional layers were frozen while the final two convolutional layers and the recurrent layer were trained on target data, following standard transfer learning practice (Du et al., 2019; Hoelzemann and Van Laerhoven, 2020). For Model A1, pre-trained models were retrained on target datasets (Kwon et al., 2020).

As a fourth bias mitigation approach, we investigated whether transfer learning from foundation models (models pretrained on large-scale, diverse population data) could reduce bias in FOG detection. We hypothesized that rich

**TABLE 2** Median values for continuous subject attributes

Attribute	Daphnet	De Souza	tDCS FOG	DeFOG
Age (years)	66	69	69	69
Disease Duration (years)	12.5	7	9	13

activity representations learned from broader populations would transfer more equitably across demographic groups than models trained solely on limited FOG datasets. We evaluated two foundation model approaches that differed in their pretraining strategies and architectures: Model B1 pretrained via self-supervised learning on 700,000 person-days of wrist-worn accelerometer data from 100,000 UK Biobank participants (Doherty et al., 2017; Yuan et al., 2024), and Model B2, which uses a transformer architecture pretrained on accelerometer data from 29,307 National Health and Nutrition Examination Survey (NHANES) participants (Centers for Disease Control and Prevention and others, 2019; Ruan et al., 2025). For Model B1, we selected the variant trained on 5-second windows to match our FOG detection window length (3-5 seconds), modified only the output layer for binary FOG classification, and fine-tuned all layers during training on the four FOG datasets (Yuan et al., 2024). For Model B2, we hypothesized that its transformer architecture for modeling long-range temporal dependencies (Vaswani et al., 2017), combined with pretraining on demographically diverse NHANES data, would yield robust representations transferable to FOG detection. To adapt the multi-channel FOG sensor data to Model B2's single-channel input requirement, we selected one sensor location per dataset and computed the magnitude from tri-axial accelerometer channels (Ruan et al., 2025). We froze all pretrained backbone weights and fine-tuned only the final classification layer on each FOG dataset (Du et al., 2019; Hoelzemann and Van Laerhoven, 2020).

## 2.6 | Model Performance and Bias Evaluation

All models were evaluated using macro F1-scores under user-independent cross-validation to account for substantial class imbalance and ensure generalization to unseen subjects (Opitz and Burst, 2021; Kwon et al., 2019). The macro F1-score treats each class equally by computing the F1-score for each class independently, then averaging:

$$F1 = \frac{2}{|c|} \sum_c \frac{prec_c \times recall_c}{prec_c + recall_c}$$

where  $|c|$  is the number of FOG classes, and  $prec_c$  and  $recall_c$  are the precision and recall for each class respectively (Opitz and Burst, 2021). In clinical terms, recall represents sensitivity (the proportion of true FOG episodes correctly detected), while precision represents positive predictive value (the proportion of detected episodes that are truly FOG). DeFOG, tDCS FOG, and De Souza datasets were evaluated using 5-fold user-independent cross-validation, while Daphnet used 3-fold user-independent cross-validation. Fewer folds for Daphnet (10 subjects) ensured each test fold included representation from both groups within each protected attribute (e.g., both male and female subjects for the sex attribute) for fairness evaluation. Accounting for randomness in data splits and model training, we ran 10 iterations of cross-validation and reported average F1-scores across all test folds with 95% confidence intervals for statistical significance.

Following standard group fairness evaluation (Dwork et al., 2012; Hardt et al., 2016), we assessed whether models achieved comparable performance across subject groups defined by protected attributes (FOG phenotype, sex,

age, disease duration). As shown in Figure 1, subjects in each dataset were stratified into two groups per protected attribute. To assess fairness across FOG phenotypes, episodes were classified as tremulous or akinetic based on spectral analysis of accelerometer data (Moore et al., 2013). Episodes with total power in the freezing band (3-8 Hz) exceeding that in the locomotion band (0-3 Hz) were classified as tremulous; remaining episodes were classified as akinetic (Moore et al., 2013). For sex, we used the self-reported labels provided in the datasets (i.e., male and female). Continuous attributes (age and disease duration) were dichotomized at dataset-specific medians following standard biostatistics practice (Gong et al., 2023), as shown in Table 2.

Fairness was assessed using standard Fair ML metrics: Demographic Parity Ratio (DPR; Eq. (1)) and Equalized Odds Ratio (EOR; Eq. (3)) for most attributes (Agarwal et al., 2018), and Equality of Opportunity Difference (EOD; Eq. (2)) specifically for FOG phenotype (Hardt et al., 2016). DPR was computed for FOG phenotype, age, sex, and disease duration, while EOR was computed for age, sex, and disease duration only. For the FOG phenotype, EOD was used instead of EOR because false positive rates cannot be computed given that FOG phenotype annotation is conditional on FOG episodes being present (Moore et al., 2013). Similar to the F1-score, we reported the average DPR, EOR, and EOD, with 95% confidence intervals from 10 iterations of cross-validation, to assess the statistical significance of model bias and our bias mitigation approaches.

For rigorous statistical significance testing, we employed the Wilcoxon signed-rank test to assess whether bias mitigation strategies produced statistically significant improvements in model performance (F1-score) and fairness metrics (DPR, EOR, and EOD) (Wilcoxon, 1945). This non-parametric test was selected because it handles paired samples without requiring normality assumptions and is known to perform reliably with small sample sizes (Wilcoxon, 1945). Since we focused on evaluating improvements in performance and fairness, a one-sided test was performed with the null hypothesis that median differences were zero, and significance was determined at  $\alpha = 0.05$  (Wilcoxon, 1945). These comparisons evaluated model performance and fairness before and after applying bias mitigation methods (threshold optimization, adversarial debiasing, and multi-site transfer), as well as the effect of fine-tuning large-scale pretrained models (Models B1-B2) relative to the baseline model (Model A2).

In the absence of FOG or PD-specific fairness thresholds, we adopted the four-fifths rule (threshold = 0.8), an established threshold from the U.S. Equal Employment Opportunity Commission that is widely used in Fair ML (U.S. Equal Employment Opportunity Commission, 2023), where DPR = 1 and EOR = 1 represent perfect fairness.

## 3 | RESULTS

In this section, we first report baseline model performance and fairness metrics, then evaluate the impact of the bias mitigation approaches.

### 3.1 | Model Performance and Bias without Bias Mitigation

Model performance improved with architectural complexity across the multi-site datasets, as shown in Table 6 and Figure 2. Model A1 achieved an average F1-score of 0.578, while the deep learning architectures demonstrated superior performance: Model A2 achieved 0.682, and Model A3 achieved 0.688. This progression reflected the increasing capacity of these architectures to capture temporal dependencies in wearable sensor data, with the attention-based Model A3 providing marginal gains over the convolutional-recurrent approach of Model A2.

Despite these performance gains, all models exhibited suboptimal fairness across clinical and demographic attributes, with no model achieving the 0.8 four-fifths rule threshold for any fairness metric (Table 6). FOG phenotype

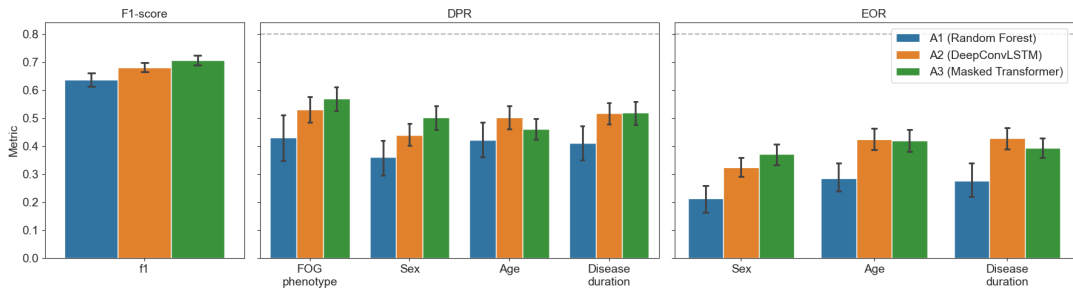


**FIGURE 2** Mean F1-score, Demographic Parity Ratio (DPR), and Equalized Odds Ratio (EOR) for each model across the multi-site datasets prior to applying bias mitigation approaches. Error bars indicate the 95% confidence intervals. Dashed horizontal lines represent the fairness threshold (0.8 for DPR and EOR).

bias was particularly pronounced: DPR ranged from 0.435 (Model A1) to 0.540 (Model A3), and EOD ranged from 0.119 to 0.233, indicating systematic underperformance on underrepresented FOG phenotypes. Demographic attributes showed comparable fairness, with sex-based DPR values between 0.413 and 0.514, age-based DPR between 0.463 and 0.486, and disease duration-based DPR between 0.429 and 0.509. EOR values were consistently low, with all values below 0.42 across protected attributes. Critically, increased model performance did not correspond to improved fairness, suggesting that standard training procedures introduced systematic biases that require targeted mitigation.

### 3.2 | Model Performance and Bias with Bias Mitigation

Bias mitigation strategies yielded variable results, with most approaches failing to meet fairness thresholds across all attributes, including the FOG phenotype. Threshold optimization for Model A1 showed mixed outcomes with minimal performance impact (DPR: -0.126, EOR: +0.063, F1-score: -0.011), while adversarial debiasing applied independently to each attribute yielded mixed results for both Model A2 (DPR: +0.005, EOR: -0.014, F1-score: -0.011) and Model A3 (DPR: -0.002, EOR: -0.021, F1: -0.017) models. For FOG phenotype specifically, independent adversarial debiasing increased DPR by +0.048 (Model A2) and +0.035 (Model A3), though both remained well below fairness thresholds. Multi-head adversarial debiasing produced negligible overall changes in fairness metrics for both architectures (DPR: +0.002, EOR: +0.007).

Transfer learning approaches substantially outperformed other mitigation strategies in both fairness gains and performance improvements, although fairness thresholds were not met. Multi-site transfer learning increased F1-scores by +0.024 (Model A2) and +0.017 (Model A3), while improving DPR (+0.037) and EOR (+0.045) for both architectures. For the FOG phenotype, DPR improved by +0.051 (Model A2) and +0.045 (Model A3), respectively. Transfer learning from generic activity representations (Model B1) improved F1-scores (+0.015) and DPR (+0.027) but showed minimal improvement for FOG phenotype (DPR: +0.002).

Fine-tuning Model B2 produced the largest fairness gains, increasing DPR by +0.159 and EOR by +0.131 across all attributes, including FOG phenotype (DPR: +0.157), though this came at a substantial performance cost (F1-score: -0.074) and still fell short of fairness thresholds. The improvements were consistent across demographic attributes, with DPR gains of +0.156 for sex, +0.167 for age ( $p < 0.05$ ), and +0.155 for disease duration ( $p < 0.05$ ), and EOR improvements ranging from +0.123 to +0.146. Despite representing the strongest fairness improvements among all tested approaches, most attributes remained below the four-fifths rule threshold across datasets.

Notably, the only experiment we conducted in which bias mitigation reduced bias to meet the four-fifths rule

**TABLE 3** Average change in performance (F1-score) and fairness (DPR, EOR, and EOD) across multi-site datasets after applying bias mitigation approaches (shown in the Bias Mitigation column). Statistical significance of changes was assessed using paired Wilcoxon signed-rank tests across datasets, comparing baseline and mitigation models. Each metric was first averaged within each dataset, and the Wilcoxon test was applied to these dataset-level averages to assess independence between pairs (Asterisks indicate significance levels: \*  $p < 0.1$ , \*\*  $p < 0.05$ ).

Bias Mitigation	Model	$\Delta F1\text{-score}$	$\Delta DPR$ (all attributes)	$\Delta EOR$ (Sex, Age, Disease duration)	$\Delta DPR$ FOG phenotype	$\Delta EOD$ FOG phenotype	$\Delta DPR$ Sex	$\Delta DPR$ Age	$\Delta DPR$ Disease duration	$\Delta EOR$ Sex	$\Delta EOR$ Age	$\Delta EOR$ Disease duration
Threshold optimizer	A1	-0.011	-0.126	+0.063	+0.017	+0.017	-0.096	-0.221	-0.207	+0.072	+0.059	+0.060
Adversarial debiasing (Single attribute)	A2	-0.011	+0.005	-0.014	+0.048	-0.003	+0.031	-0.019	-0.018	+0.036	-0.008	-0.009
	A3	-0.017	-0.002	-0.021	+0.035	0.000	-0.060	+0.017	+0.007	-0.067	-0.001	+0.003
Adversarial debiasing (Multi-Head MLP)	A2	+0.001	-0.019	-0.011	-0.001	+0.015	-0.002	-0.033	-0.029	+0.004	-0.002	-0.033
	A3	-0.032	+0.002	+0.007	+0.047	-0.020	-0.062	+0.087	-0.019	-0.027	+0.052	-0.002
Multi-site Transfer	A1	-0.010	-0.017	-0.022	-0.038	-0.004	+0.021	-0.080	+0.026	-0.018	-0.014	-0.035
	A2	+0.024	+0.037	0.045	+0.051	+0.028	+0.038	+0.043	+0.016	+0.062*	-0.041	+0.033
	A3	+0.017	+0.037	0.045	+0.045	+0.031	-0.012	+0.045*	+0.021	+0.023	+0.058	+0.047
Generic Activity Feature Transfer	B1	+0.015	+0.027	-0.005	+0.002	+0.030	+0.056	+0.022	+0.027	+0.022	-0.025	-0.012
Foundation Model Feature Transfer	B2	-0.074	+0.159	+0.131	+0.157	-0.010	+0.156	+0.167*	+0.155*	+0.146	+0.125	+0.123

was Model B2 (foundation model feature transfer) on the tDCS FOG dataset. This approach achieved DPR values exceeding 0.80 for all protected attributes (sex: 0.855, age: 0.820, disease duration: 0.850, FOG phenotype: 0.939), though at the cost of reduced F1-score (0.558 vs. 0.722 baseline).

Bias mitigation results are summarized in Table 3, with detailed performance (F1-score) and fairness metrics (DPR, EOR, and EOD) for all approaches shown in Table 4. Results for fine-tuning large-scale pretrained models for human activity are presented separately in Table 5.

## 4 | DISCUSSION

The main contribution of this work was the application of fair machine learning concepts to demonstrate systematic differences in FOG detection performance across FOG phenotypes and demographic strata. We found that conventional bias mitigation techniques showed limited effectiveness, whereas multi-site transfer learning showed the most promise for reducing bias and improving overall performance. Our findings underscore systematic performance differences across FOG phenotypes, with the majority of models failing to meet fairness thresholds regardless of mitigation approach. Across majority datasets and experiments, DPR for FOG phenotypes remained below 0.8, indicating persistent bias favoring one phenotype over the other. This finding aligns with prior work by Yang et al. (2024), who reported that FOG detection models showed higher agreement with expert raters for tremulous FOG compared to akinetic FOG.

These findings suggest that post hoc algorithmic corrections alone, while helpful, may be inadequate when underlying data imbalance and phenotype heterogeneity are substantial. Critically, all bias mitigation approaches, including both conventional and transfer learning-based methods, failed to eliminate these phenotype-based disparities. Future efforts may require intentional sampling strategies that explicitly enrich underrepresented FOG phenotypes and demographic subgroups during data collection. This persistence suggests the performance differences arise from genuine pathophysiological differences in motor mechanisms between phenotypes (Factor et al., 2025). Such approaches could improve representation at the data level rather than relying solely on downstream mitigation. An alternative

or complementary strategy may be the development of phenotype-specific or stratified models, in which separate models are trained for distinct FOG manifestations. This may allow models to better capture phenotype-dependent signal characteristics that are otherwise obscured in pooled training.

#### 4.1 | Model Performance and Bias without Bias Mitigation

Deep learning architectures substantially outperformed shallow ML architectures for FOG detection across all datasets, with Model A2-A3 achieving macro-F1 scores that were +0.104 and +0.110 higher than Model A1, respectively. This aligned with prior work by Kwon *et al.* (Kwon *et al.*, 2019), which demonstrated superior FOG detection performance for deep learning architectures compared to shallow machine learning models by capturing temporal dependencies related to FOG. The highest performance (macro F1-score of 0.778) was achieved on the De Souza dataset, likely due to its simpler protocol, which focused on turning (Ribeiro De Souza *et al.*, 2022), in comparison to the more complex protocols in other datasets (e.g., walking, sitting, standing, opening doors).

Without bias mitigation, no protected attribute was found fair across the four datasets ( $DPR \leq 0.8$ ). The tDCS FOG dataset had the highest DPR and EOR values across most protected attributes, with DPRs of 0.622, 0.677, and 0.715 and EORs of 0.561, 0.684, and 0.624 for sex, age, and disease duration, respectively. This relatively better performance likely resulted from the tDCS FOG dataset's larger sample size ( $N=62$ ), which provided greater representation compared to other datasets. These findings demonstrated that adequate data representation is critical for bias mitigation.

More critically, the FOG phenotype showed bias ( $DPR < 0.8$ ) across all datasets and models, due to significantly fewer akinetic than tremulous FOG episodes. This imbalance reflected documented FOG phenotype distributions, as akinetic FOG occurs less frequently than tremulous FOG (Zoetewei *et al.*, 2025), requiring more specific triggers (e.g., gait initiation) versus the more readily occurring tremulous episodes during general motion.

#### 4.2 | Model Performance and Bias with Bias Mitigation

The conventional bias mitigation approaches (i.e., threshold optimization, adversarial debiasing) yielded expected performance trade-offs, showing modest decreases in F1 score across models ( $-0.032$  to  $-0.010$ ). These reductions align with established findings in Fair ML literature: fairness constraints force models away from performance-optimal solutions by either imposing group-dependent decision thresholds (threshold optimization) or suppressing predictive information correlated with protected attributes (adversarial debiasing) (Hardt *et al.*, 2016; Zhang *et al.*, 2018; Menon and Williamson, 2018)

In contrast, two transfer learning approaches improved model performance while mitigating bias, with multi-site transfer yielding an average increase in F1 score of +0.020 and generic activity feature transfer increasing scores by +0.015. Multi-site transfer leveraged the diversity across FOG datasets, exposing models to varied patient populations, sensor configurations, and clinical protocols during pretraining. This cross-dataset exposure enabled models to learn robust FOG representations that generalize beyond site-specific characteristics, reducing overfitting to the demographic and clinical distributions of any single dataset. The increase in F1-score with Model B1 (+0.015) was consistent with the work by Yuan *et al.* (2024), who reported that their large generic activity recognition model was useful even in downstream health applications.

Despite testing multiple bias mitigation approaches, none met the fairness threshold, with only transfer learning methods showing meaningful fairness improvements. Conventional bias mitigation techniques showed limited effectiveness, both producing mixed results across fairness metrics: threshold optimization with Model A1 ( $-0.126$  DPR,

+0.063 EOR), and single-attribute adversarial debiasing with Models A2-A3 (+0.002 DPR, -0.018 EOR). In contrast, transfer learning approaches leveraged diverse, large-scale datasets to improve both fairness and performance, with multi-site transfer with Model A2-A3 (+0.037 DPR, +0.045 EOR) and generic activity feature transfer in Model B1 (+0.027 DPR) demonstrating that richer training data reduced bias. Only one mitigation approach met the fairness threshold: transfer learning from Model B2 on one dataset (tDCS FOG), but at a substantial performance cost (a -0.164 decrease in F1-score). Model B2's pretraining on the demographically diverse NHANES dataset likely enabled learning of demographic-invariant features, improving fairness but suppressing clinically relevant features specific to FOG detection.

#### 4.3 | Relation to Current State of the Art

Our models represent the state of the art in FOG detection when compared with successful solutions from the Kaggle Freezing of Gait detection challenge, which introduced the DeFOG and tDCS FOG datasets used in this study (Salomon et al., 2024; Howard et al., 2023). Model A3 (Masked Transformer) with multi-site transfer, pretrained on DeFOG and Daphnet and finetuned on tDCS FOG, achieved performance comparable to the competition's first-place solution (Model A3 F1-score = 0.762 versus first-place F1-score = 0.790) (Salomon et al., 2024). Both approaches relied on transformer architectures that model temporal dependencies in FOG episodes (Vaswani et al., 2017). We evaluated our models using cross-validation on the public training data from the challenge rather than on the private test set used to rank competition submissions, limiting direct comparison with leaderboard results. Additionally, the challenge leaderboard scored models using both F1-score and Mean Average Precision across FOG event classes (e.g., turn, start hesitation, walking) (Salomon et al., 2024), whereas we evaluated binary FOG detection using F1-score alone. Nevertheless, since our models achieved state-of-the-art performance, the fairness analysis framework presented here could be applied to evaluate bias in competition-winning solutions.

#### 4.4 | Limitations and Future Work

While transfer learning approaches showed promise for improving both performance and fairness, several limitations warrant consideration.

Based on the data we used here, we can speculate on the future of the state of the art. In particular, the foundation models (Model B1 and B2) were not necessarily trained on subjects with movement disorders, creating a domain gap between the pretraining data and the clinical FOG detection task (Wiggins and Tejani, 2022). Foundation models trained specifically on movement disorders populations could better capture the motor symptom heterogeneity characteristics of FOG and PD, potentially improving both fairness and performance. Such disease-specific pretraining may be essential for achieving consistent FOG detection across diverse patient populations with different phenotypes and demographics.

This study evaluated fairness with respect to individual attributes (FOG phenotype, sex, age, disease duration) but did not examine intersectional biases arising from combinations of protected attributes. However, clinical evidence demonstrates that protected attributes interact to influence PD and FOG presentation, such as women developing PD at later ages than men (Macht et al., 2007; Fullard et al., 2018). Future work may employ intersectional fairness frameworks (Wang et al., 2022; Lett and La Cava, 2023) to evaluate model performance across multi-attribute patient groups and address biases.

We used dataset-specific optimal temporal window sizes from prior literature rather than a unified optimal window, which may have limited cross-dataset methodological consistency (Bächlin et al., 2010; Reches et al., 2020).

Particularly, different window sizes may capture FOG phenotypes differently, with shorter windows potentially favoring brief akinetic episodes and longer windows favoring sustained tremulous freezing. Future work may develop a data-driven approach to identify a single optimal temporal window size that generalizes across FOG phenotypes and datasets.

## 5 | CONCLUSION

Freezing of gait (FOG) is a debilitating symptom of Parkinson's disease that is challenging to capture during clinical assessments, creating a need for wearable-based continuous monitoring. However, for such systems to expand specialist care equitably, models must perform consistently across FOG phenotypes and demographics. This work provides the first systematic evaluation of bias and fairness in wearable-based FOG detection, evaluating state-of-the-art models and bias mitigation approaches (threshold optimization, adversarial debiasing, transfer learning) across multi-site datasets. Our findings revealed performance differences across FOG phenotypes and demographic groups, with models frequently failing to meet the established four-fifths fairness threshold. While conventional mitigation approaches improved fairness, they did not do so consistently. Transfer learning using multi-site data and large-scale pretrained (foundation) models was more effective, though foundation models required performance trade-offs to achieve fairness thresholds. Critically, the FOG phenotype emerged as a significant source of bias, with akinetic episodes substantially underrepresented in datasets and associated with performance disparities, with direct implications for clinical care. These findings show that achieving equitable FOG detection requires proactive considerations during data collection, including stratified sampling by phenotype and demographics, rather than relying solely on bias mitigation approaches.

## References

Tariq Adnan, Md Saiful Islam, Sangwu Lee, EM Wasifur Rahman Chowdhury, Sutapa Dey Tithi, Kazi Noshin, Md Rayhanul Islam, Imran Sarker, M Saifur Rahman, Ruth B Schneider, et al. Ai-enabled parkinson's disease screening using smile videos. *NEJM AI*, 2(7):Aloa2400950, 2025.

Alekh Agarwal, Alina Beygelzimer, Miroslav Dudik, John Langford, and Hanna Wallach. A Reductions Approach to Fair Classification. In Jennifer Dy and Andreas Krause, editors, *Proceedings of the 35th International Conference on Machine Learning*, volume 80 of *Proceedings of Machine Learning Research*, pages 60–69, Vancouver, Canada, 10–15 Jul 2018. PMLR. URL <https://proceedings.mlr.press/v80/agarwal18a.html>.

Marc Bächlin, Meir Plotnik, Daniel Roggen, Inbal Maidan, Jeffrey M. Hausdorff, Nir Giladi, and Gerhard Tröster. Wearable assistant for parkinson's disease patients with the freezing of gait symptom. *Trans. Info. Tech. Biomed.*, 14(2):436–446, Mar 2010. ISSN 1089-7771. doi: 10.1109/TITB.2009.2036165. URL <https://doi-org.proxy.library.emory.edu/10.1109/TITB.2009.2036165>.

Claudia Barthel, Elizabeth Mallia, Bettina Debū, Bastiaan R Bloem, and Murielle Ursulla Ferraye. The Practicalities of Assessing Freezing of Gait. *Journal of Parkinson's Disease*, 6(4):667–674, 2016.

Leo Breiman. Random forests. *Machine Learning*, 45:5–32, 2001.

Andreas Bulling, Ulf Blanke, and Bernt Schiele. A tutorial on human activity recognition using body-worn inertial sensors. *ACM Computing Surveys (CSUR)*, 46(3):1–33, 2014.

Centers for Disease Control and Prevention and others. Nhanes-national health and nutrition examination survey homepage. *National Center for Health Statistics*, 2019.

Avijoy Chakma, Abu Zaher Md Faridee, Md Abdullah Al Hafiz Khan, and Nirmalya Roy. Activity recognition in wearables using adversarial multi-source domain adaptation. *Smart Health*, 19:100174, 2021.

Richard J Chen, Judy J Wang, Drew FK Williamson, Tiffany Y Chen, Jana Lipkova, Ming Y Lu, Sharifa Sahai, and Faisal Mahmood. Algorithm fairness in artificial intelligence for medicine and healthcare. *Nature Biomedical Engineering*, 7(6):719–742, June 2023. doi: 10.1038/s41551-023-01056-8.

Aiden Doherty, Dan Jackson, Nils Hammerla, Thomas Plötz, Patrick Olivier, Malcolm H Granat, Tom White, Vincent T Van Hees, Michael I Trenell, Christopher G Owen, et al. Large scale population assessment of physical activity using wrist worn accelerometers: the uk biobank study. *PLOS One*, 12(2):e0169649, 2017.

Xin Du, Katayoun Farahi, and Mahesan Niranjan. Transfer learning across human activities using a cascade neural network architecture. In *Proceedings of the 2019 ACM International Symposium on Wearable Computers*, ISWC '19, page 35–44, New York, NY, USA, 2019. Association for Computing Machinery. ISBN 9781450368704. doi: 10.1145/3341163.3347730. URL <https://doi-org.proxy.library.emory.edu/10.1145/3341163.3347730>.

Cynthia Dwork, Moritz Hardt, Toniann Pitassi, Omer Reingold, and Richard Zemel. Fairness through awareness. In *Proceedings of the 3rd Innovations in Theoretical Computer Science Conference*, ITCS '12, page 214–226, New York, NY, USA, 2012. Association for Computing Machinery. ISBN 9781450311151. doi: 10.1145/2090236.2090255. URL <https://doi-org.proxy.library.emory.edu/10.1145/2090236.2090255>.

Stewart A Factor, David Weinshenker, and J Lucas McKay. A possible pathway to freezing of gait in parkinson's disease. *Journal of Parkinson's Disease*, 15(2):282–290, 2025.

Emilio Ferrara. Fairness and bias in artificial intelligence: A brief survey of sources, impacts, and mitigation strategies. *Sci*, 6(1):3, 2023.

Benjamin Filtjens, Pieter Ginis, Alice Nieuwboer, Peter Slaets, and Bart Vanrumste. Automated freezing of gait assessment with marker-based motion capture and multi-stage spatial-temporal graph convolutional neural networks. *Journal of NeuroEngineering and Rehabilitation*, 19(1):48, 2022.

Michelle E Fullard, Dylan P Thibault, Veronica Todaro, Susan Foster, Lori Katz, Robin Morgan, Drew S Kern, Jason M Schwalb, Enrique Urrea Mendoza, Nabila Dahodwala, et al. Sex disparities in health and health care utilization after parkinson diagnosis: Rethinking pd associated disability. *Parkinsonism & related disorders*, 48:45–50, 2018.

Moran Gilat, Jorik Nonnikes, Stewart A. Factor, Bastiaan R. Bloem, John G. Nutt, Nir Giladi, Mark Hallett, Alice Nieuwboer, Fay B. Horak, Daniel Weiss, Esther Cubo, Demi Zoetewei, Caroline Moreau, Beomseok Jeon, Tuhin Virmani, Jeffrey M. Hausdorff, Alfonso Fasano, Simon J. G. Lewis, and International Consortium for Freezing of Gait. An updated definition of freezing of gait. *Nature Reviews Neurology*, jan 2026. doi: 10.1038/s41582-025-01179-3. URL <https://doi.org/10.1038/s41582-025-01179-3>. Published online 09 January 2026.

N. Jabin Gong, Gari D. Clifford, Christine D. Esper, Stewart A. Factor, J. Lucas McKay, and Hyeokhyen Kwon. Classifying tremor dominant and postural instability and gait difficulty subtypes of parkinson's disease from full-body kinematics. *Sensors*, 23:8330, 10 2023. ISSN 14248220. doi: 10.3390/s23198330.

Mark Hallett. The intrinsic and extrinsic aspects of freezing of gait. *Movement Disorders*, 23(S2):S439–S443, 2008.

Nils Y. Hammerla, Reuben Kirkham, Peter Andras, and Thomas Ploetz. On preserving statistical characteristics of accelerometry data using their empirical cumulative distribution. In *Proceedings of the 2013 International Symposium on Wearable Computers*, ISWC '13, page 65–68, New York, NY, USA, 2013. Association for Computing Machinery. ISBN 9781450321273. doi: 10.1145/2493988.2494353. URL <https://doi-org.proxy.library.emory.edu/10.1145/2493988.2494353>.

Moritz Hardt, Eric Price, and Nathan Srebro. Equality of opportunity in supervised learning. In *Proceedings of the 30th International Conference on Neural Information Processing Systems*, NIPS'16, page 3323–3331, Red Hook, NY, USA, 2016. Curran Associates Inc. ISBN 9781510838819.

Harish Haresamudram, Apoorva Beedu, Varun Agrawal, Patrick L. Grady, Irfan Essa, Judy Hoffman, and Thomas Plötz. Masked reconstruction based self-supervision for human activity recognition. In *Proceedings of the 2020 ACM International Symposium on Wearable Computers, ISWC '20*, page 45–49, New York, NY, USA, 2020. Association for Computing Machinery. ISBN 9781450380775. doi: 10.1145/3410531.3414306. URL <https://doi.org/10.1145/3410531.3414306>.

Kaiming He, Xiangyu Zhang, Shaoqing Ren, and Jian Sun. Deep residual learning for image recognition. In *2016 IEEE Conference on Computer Vision and Pattern Recognition (CVPR)*, pages 770–778, Las Vegas, NV, USA, 2016. IEEE. doi: 10.1109/CVPR.2016.90.

Alexander Hoelzemann and Kristof Van Laerhoven. Digging deeper: towards a better understanding of transfer learning for human activity recognition. In *Proceedings of the 2020 ACM International Symposium on Wearable Computers, ISWC '20*, page 50–54, New York, NY, USA, 2020. Association for Computing Machinery. ISBN 9781450380775. doi: 10.1145/3410531.3414311. URL <https://doi-org.proxy.library.emory.edu/10.1145/3410531.3414311>.

Addison Howard, Amit Salomon, Eran Gazit, Jeff Hausdorff, HCL Jevster, Leslie Kirsch, Pieter Ginis Maggie, Ryan Holbrook, and Karim F Yasir. Parkinson's freezing of gait prediction, 2023. URL <https://kaggle.com/competitions/tlvmc-parkinsons-freezing-gait-prediction>.

Preeti Khera and Neelesh Kumar. Age-gender specific prediction model for parkinson's severity assessment using gait biomarkers. *Engineering Science and Technology, an International Journal*, 27:101005, 2022.

Peter J Koehler, Jorik Nonnikes, and Bastiaan R Bloem. Freezing of gait before the introduction of levodopa. *The Lancet Neurology*, 20(2):97, 2021.

Essodjolo Kpatcha. Balancing fairness and accuracy in machine learning-based probability of default modeling via threshold optimization. *Journal of Risk and Financial Management*, 18(12):724, 2025.

Hyekhyen Kwon, Gregory D. Abowd, and Thomas Plötz. Handling annotation uncertainty in human activity recognition. In *Proceedings of the 2019 ACM International Symposium on Wearable Computers, ISWC '19*, page 109–117, New York, NY, USA, 2019. Association for Computing Machinery. ISBN 9781450368704. doi: 10.1145/3341163.3347744. URL <https://doi-org.proxy.library.emory.edu/10.1145/3341163.3347744>.

Hyekhyen Kwon, Catherine Tong, Harish Haresamudram, Yan Gao, Gregory D Abowd, Nicholas D Lane, and Thomas Ploetz. Imutube: Automatic extraction of virtual on-body accelerometry from video for human activity recognition. *Proceedings of the ACM on Interactive, Mobile, Wearable and Ubiquitous Technologies*, 4(3):1–29, 2020.

Hyekhyen Kwon, Gari D. Clifford, Imari Genias, Doug Bernhard, Christine D. Esper, Stewart A. Factor, and J. Lucas McKay. An explainable spatial-temporal graphical convolutional network to score freezing of gait in parkinsonian patients. *Sensors*, 23(4), 2023. ISSN 1424-8220. doi: 10.3390/s23041766. URL <https://www.mdpi.com/1424-8220/23/4/1766>.

Elle Lett and William G La Cava. Translating intersectionality to fair machine learning in health sciences. *Nature Machine Intelligence*, 5(5):476–479, 2023.

Johannes Link, Timur Perst, Maike Stoeve, and Bjoern M Eskofier. Wearable sensors for activity recognition in ultimate frisbee using convolutional neural networks and transfer learning. *Sensors*, 22(7):2560, 2022.

Michael Macht, Yvonne Kaussner, Jens Carsten Möller, Karin Stiasny-Kolster, Karla Maria Eggert, Hans-Peter Krüger, and Heiner Ellgring. Predictors of freezing in parkinson's disease: a survey of 6,620 patients. *Movement disorders*, 22(7):953–956, 2007.

Martina Mancini, Bastiaan R Bloem, Fay B Horak, Simon JG Lewis, Alice Nieuwboer, and Jorik Nonnikes. Clinical and methodological challenges for assessing freezing of gait: future perspectives. *Movement Disorders*, 34(6):783–790, 2019.

Martina Mancini, J. Lucas McKay, Helena Cockx, Nicholas D'Cruz, Christine D. Esper, Benjamin Filtjens, Benedetta Heimler, Colum D. MacKinnon, Luca Palmerini, Melvyn Roerdink, William R. Young, Jeffrey M. Hausdorff, and ICFOG Investigators. Technology for measuring freezing of gait: Current state of the art and recommendations. *Journal of Parkinsons Disease*, 15(1):19–40, February 2025. doi: 10.1177/1877718X241301065. URL <https://doi.org/10.1177/1877718X241301065>.

J. Lucas McKay, Felicia C. Goldstein, Barbara Sommerfeld, Douglas Bernhard, Sahyli Perez Parra, and Stewart A. Factor. Freezing of gait can persist after an acute levodopa challenge in parkinson's disease. *NPJ Parkinsons Disease*, 5:25, 2019. doi: 10.1038/s41531-019-0099-z.

Ninareh Mehrabi, Fred Morstatter, Nripsuta Saxena, Kristina Lerman, and Aram Galstyan. A survey on bias and fairness in machine learning. *ACM computing surveys (CSUR)*, 54(6):1–35, 2021.

Aditya Krishna Menon and Robert C. Williamson. The cost of fairness in binary classification. In Sorelle A. Friedler and Christo Wilson, editors, *Proceedings of the 1st Conference on Fairness, Accountability and Transparency*, volume 81 of *Proceedings of Machine Learning Research*, pages 107–118. PMLR, 23–24 Feb 2018. URL <https://proceedings.mlr.press/v81/menon18a.html>.

Aya A Mitani, Nathaniel D Mercaldo, Sebastien Haneuse, and Jonathan S Schildcrout. Survey design and analysis considerations when utilizing misclassified sampling strata. *BMC Medical Research Methodology*, 21(1):145, 2021.

Steven T Moore, Don A Yungher, Tiffany R Morris, Valentina Dilda, Hamish G MacDougall, James M Shine, Sharon L Naismith, and Simon JG Lewis. Autonomous identification of freezing of gait in parkinson's disease from lower-body segmental accelerometry. *Journal of neuroengineering and rehabilitation*, 10(1):19, 2013.

John G Nutt, Bastiaan R Bloem, Nir Giladi, Mark Hallett, Fay B Horak, and Alice Nieuwboer. Freezing of gait: moving forward on a mysterious clinical phenomenon. *The Lancet Neurology*, 10(8):734–744, 2011.

Juri Opitz and Sebastian Burst. Macro f1 and macro f1, 2021. URL <https://arxiv.org/abs/1911.03347>.

Francisco Javier Ordóñez and Daniel Roggen. Deep Convolutional and LSTM Recurrent Neural Networks for Multimodal Wearable Activity Recognition. *Sensors*, 16(1):115, 2016. ISSN 1424-8220. doi: 10.3390/s16010115. URL <https://www.mdpi.com/1424-8220/16/1/115>.

Scott Pardoel, Jonathan Kofman, Julie Nantel, and Edward D Lemaire. Wearable-sensor-based detection and prediction of freezing of gait in parkinson's disease: a review. *Sensors*, 19(23):5141, 2019.

Diane Podsiadlo and Sandra Richardson. The timed "up & go": a test of basic functional mobility for frail elderly persons. *Journal of the American geriatrics Society*, 39(2):142–148, 1991.

Tal Reches, Moria Dagan, Talia Herman, Eran Gazit, Natalia A Gouskova, Nir Giladi, Brad Manor, and Jeffrey M Hausdorff. Using wearable sensors and machine learning to automatically detect freezing of gait during a fog-provoking test. *Sensors*, 20(16):4474, 2020.

Caroline Ribeiro De Souza, Runfeng Miao, Júlia Ávila De Oliveira, Andrea Cristina De Lima-Pardini, Débora Fragoso De Campos, Carla Silva-Batista, Luis Teixeira, Solaiman Shokur, Bouri Mohamed, and Daniel Boari Coelho. A public data set of videos, inertial measurement unit, and clinical scales of freezing of gait in individuals with parkinson's disease during a turning-in-place task. *Frontiers in Neuroscience*, 16:832463, 2022.

Daniel Roggen, Alberto Calatroni, Mirco Rossi, Thomas Holleczek, Kilian Förster, Gerhard Tröster, Paul Lukowicz, David Bannach, Gerald Pirkl, Alois Ferscha, et al. Collecting complex activity datasets in highly rich networked sensor environments. In *2010 Seventh international conference on networked sensing systems (INSS)*, pages 233–240. IEEE, 2010.

Daniel Roggen, Meir Plotnik, and Jeff Hausdorff. Daphnet Freezing of Gait. UCI Machine Learning Repository, 2013. DOI: <https://doi.org/10.24432/C56K78>.

Samanta Rosati, Gabriella Balestra, and Marco Knaflitz. Comparison of different sets of features for human activity recognition by wearable sensors. *Sensors*, 18(12):4189, 2018. ISSN 1424-8220. doi: 10.3390/s18124189. URL <https://www.mdpi.com/1424-8220/18/12/4189>.

Franklin Y. Ruan, Aiwei Zhang, Jenny Y. Oh, SouYoung Jin, and Nicholas C. Jacobson. Foundation models for wearable movement data in mental health research, 2025. URL <https://arxiv.org/abs/2411.15240>.

Amit Salomon, Eran Gazit, Pieter Ginis, Baurzhan Urazalinov, Hirokazu Takoi, Taiki Yamaguchi, Shuhei Goda, David Lander, Julien Lacombe, Aditya Kumar Sinha, Alice Nieuwboer, Leslie C. Kirsch, Ryan Holbrook, Brad Manor, and Jeffrey M. Hausdorff. A machine learning contest enhances automated freezing of gait detection and reveals time-of-day effects. *Nature Communications*, 15:4853, 2024. doi: 10.1038/s41467-024-49027-0. URL <https://doi.org/10.1038/s41467-024-49027-0>.

JD Schaafsma, Y Balash, T Gurevich, AL Bartels, Jeffrey M Hausdorff, and Nir Giladi. Characterization of freezing of gait subtypes and the response of each to levodopa in Parkinson's disease. *European Journal of Neurology*, 10(4):391–398, 2003.

Ismaeel A Siddiqui, Nickolas Littlefield, Luke A Carlson, Matthew Gong, Avani Chhabra, Zoe Menezes, George M Mastorakos, Sakshi Mehul Thakar, Mehrnaz Abedian, Ines Lohse, et al. Fair ai-powered orthopedic image segmentation: addressing bias and promoting equitable healthcare. *Scientific Reports*, 14(1):16105, 2024.

Sonish Sivarajkumar, Yufei Huang, and Yanshan Wang. Fair patient model: Mitigating bias in the patient representation learned from the electronic health records. *Journal of biomedical informatics*, 148:104544, 2023.

U.S. Equal Employment Opportunity Commission. Select Issues: Assessing Adverse Impact in Software, Algorithms, and Artificial Intelligence Used in Employment Selection Procedures Under Title VII of the Civil Rights Act of 1964. [https://www.eeoc.gov/laws/guidance/select-issues-assessing-adverse-impact-software-algorithms-and-artificial#\\_ednref14](https://www.eeoc.gov/laws/guidance/select-issues-assessing-adverse-impact-software-algorithms-and-artificial#_ednref14), 2023.

Kush R. Varshney. *Trustworthy Machine Learning*. Independently published, Chappaqua, NY, USA, 2022. URL <http://trustworthymachinelearning.com>.

Ashish Vaswani, Noam Shazeer, Niki Parmar, Jakob Uszkoreit, Llion Jones, Aidan N Gomez, Łukasz Kaiser, and Illia Polosukhin. Attention is all you need. *Advances in neural information processing systems*, 30, 2017.

Sahil Verma and Julia Rubin. Fairness definitions explained. In *Proceedings of the international workshop on software fairness*, pages 1–7, 2018.

Angelina Wang, Vikram V Ramaswamy, and Olga Russakovsky. Towards intersectionality in machine learning: Including more identities, handling underrepresentation, and performing evaluation. In *Proceedings of the 2022 ACM Conference on Fairness, Accountability, and Transparency*, pages 336–349, New York, NY, USA, 2022. Association for Computing Machinery.

Hilde Weerts, Miroslav Dudík, Richard Edgar, Adrin Jalali, Roman Lutz, and Michael Madaio. Fairlearn: Assessing and improving fairness of ai systems, 2023. URL <http://jmlr.org/papers/v24/23-0389.html>.

Walter F Wiggins and Ali S Tejani. On the opportunities and risks of foundation models for natural language processing in radiology. *Radiology: Artificial Intelligence*, 4(4):e220119, 2022.

Frank Wilcoxon. Individual comparisons by ranking methods. *Biometrics bulletin*, 1(6):80–83, 1945.

Robert F Woolson. Wilcoxon signed-rank test. *Wiley encyclopedia of clinical trials*, pages 1–3, 2007.

Jenny Yang, Andrew AS Soltan, David W Eyre, and David A Clifton. Algorithmic fairness and bias mitigation for clinical machine learning with deep reinforcement learning. *Nature Machine Intelligence*, 5(8):884–894, 2023.

Po-Kai Yang, Benjamin Filtjens, Pieter Ginis, Maaike Goris, Alice Nieuwboer, Moran Gilat, Peter Slaets, and Bart Vanrumste. Automatic detection and assessment of freezing of gait manifestations. *IEEE Transactions on Neural Systems and Rehabilitation Engineering*, 2024.

Rui Yao, Guosheng Lin, Qinfeng Shi, and Damith C Ranasinghe. Efficient dense labelling of human activity sequences from wearables using fully convolutional networks. *Pattern Recognition*, 78:252–266, 2018.

Hang Yuan, Shing Chan, Andrew P Creagh, Catherine Tong, Aidan Acquah, David A Clifton, and Aiden Doherty. Self-supervised learning for human activity recognition using 700,000 person-days of wearable data. *NPJ Digital Medicine*, 7(1):91, 2024.

Piero Zappi, Clemens Lombriser, Thomas Stiefmeier, Elisabetta Farella, Daniel Roggen, Luca Benini, and Gerhard Tröster. Activity recognition from on-body sensors: accuracy-power trade-off by dynamic sensor selection. In *European Conference on Wireless Sensor Networks*, pages 17–33. Springer, 2008.

Brian Hu Zhang, Blake Lemoine, and Margaret Mitchell. Mitigating unwanted biases with adversarial learning. In *Proceedings of the 2018 AAAI/ACM Conference on AI, Ethics, and Society*, AIES '18, page 335–340, New York, NY, USA, 2018. Association for Computing Machinery. ISBN 9781450360128. doi: 10.1145/3278721.3278779. URL <https://doi-org.proxy.library.emory.edu/10.1145/3278721.3278779>.

Hanrui Zhang, Kaiwen Deng, Hongyang Li, Roger L Albin, and Yuanfang Guan. Deep learning identifies digital biomarkers for self-reported parkinson's disease. *Patterns*, 1(3), 2020.

Kerstin Ziegler, Frauke Schroeteler, Andres O Ceballos-Baumann, and Urban M Fietzek. A new rating instrument to assess festination and freezing gait in parkinsonian patients. *Movement Disorders*, 25(8):1012–1018, 2010.

Demi Zoetewei, Pieter Ginis, Talia Herman, Moran Gilat, Nicholas D'Cruz, Luca Palmerini, Eran Gazit, Jeffrey M Hausdorff, and Alice Nieuwboer. The effects of dopaminergic medication and task load on trembling and akinetic freezing of gait in parkinson's disease. *Journal of Neurology*, 272(4):296, 2025.

**TABLE 4** Model performance and fairness of the trained models for the FOG detection task. Multi-site transfer occurs when models are pretrained on source datasets (in the Pretrain dataset column). **Bold** text indicates the best value in each column for each dataset. \* indicates statistical significance ( $p \leq 0.05$ , Wilcoxon Signed Rank test (Woolson, 2007)) comparing each bias mitigation method to its corresponding no-mitigation baseline (×) within the same model and dataset.

Dataset	Model	Bias mitigation	Pretrain dataset	F1-score	Demographic Parity Ratio (DPR)				Equalized Odds Ratio (EOR)			Equality of Opportunity Difference (EOD)
					Sex	Age	Disease duration	FOG phenotype	Sex	Age	Disease duration	
DeFOG	A1	×	-	0.511 ± 0.008	0.332 ± 0.347	0.512 ± 0.311	0.279 ± 0.276	<b>0.574 ± 0.212</b>	0.141 ± 0.160	0.219 ± 0.205	0.203 ± 0.289	<b>0.027 ± 0.019</b>
		Threshold optimizer	-	0.509 ± 0.004	0.288 ± 0.108	0.349 ± 0.114	0.374 ± 0.126	0.489 ± 0.124	0.256 ± 0.108	0.283 ± 0.124	0.216 ± 0.070	0.035 ± 0.039
		Multi-site Transfer	tDCS FOG + Daphnet	0.511 ± 0.008	0.213 ± 0.239	0.260 ± 0.201	0.261 ± 0.199	0.524 ± 0.272	0.109 ± 0.187	0.096 ± 0.132	0.081 ± 0.115	0.027 ± 0.019
	A2	×	-	0.582 ± 0.010	0.402 ± 0.068	0.528 ± 0.076	0.569 ± 0.077	0.418 ± 0.064	0.300 ± 0.054	0.320 ± 0.058	0.382 ± 0.064	0.183 ± 0.027
		Adversarial debiasing (Single attribute)	-	0.575 ± 0.009	0.391 ± 0.090	0.406 ± 0.101	0.461 ± 0.086	0.422 ± 0.080	0.287 ± 0.075	0.270 ± 0.074	0.348 ± 0.089	0.152 ± 0.036
		Adversarial debiasing (Multi-Head MLP)	-	0.584 ± 0.017	0.482 ± 0.101	0.353 ± 0.088	0.428 ± 0.106	0.402 ± 0.099	0.346 ± 0.087	0.241 ± 0.069	0.280 ± 0.085	0.173 ± 0.042
	A3	Multi-site Transfer	tDCS FOG + Daphnet	0.644 ± 0.012 <sup>*</sup>	0.486 ± 0.073 <sup>*</sup>	<b>0.556 ± 0.068</b>	0.562 ± 0.071	0.494 ± 0.058 <sup>*</sup>	0.356 ± 0.055	0.429 ± 0.069 <sup>*</sup>	0.465 ± 0.068 <sup>*</sup>	0.256 ± 0.035
		Adversarial debiasing (Single attribute)	-	0.598 ± 0.014	<b>0.620 ± 0.070</b>	0.505 ± 0.078	<b>0.618 ± 0.077</b>	0.467 ± 0.068	<b>0.426 ± 0.071</b>	0.369 ± 0.071	0.393 ± 0.057	0.188 ± 0.031
		Adversarial debiasing (Multi-Head MLP)	-	0.592 ± 0.010	0.553 ± 0.118	0.486 ± 0.112	0.572 ± 0.089	0.471 ± 0.108	0.289 ± 0.086	0.317 ± 0.097	0.367 ± 0.077	0.177 ± 0.051
	A4	Multi-site Transfer	tDCS FOG + Daphnet	0.631 ± 0.011	0.560 ± 0.050	0.504 ± 0.057	0.561 ± 0.053	0.546 ± 0.053	0.415 ± 0.049	0.383 ± 0.049	0.372 ± 0.052	0.221 ± 0.030
		×	-	0.515 ± 0.006	0.622 ± 0.144	<b>0.677 ± 0.072</b>	<b>0.715 ± 0.071</b>	0.610 ± 0.124	0.487 ± 0.180	0.586 ± 0.072	0.524 ± 0.099	0.066 ± 0.024
		Threshold optimizer	-	0.519 ± 0.006	0.573 ± 0.147	0.189 ± 0.032	0.175 ± 0.033	0.702 ± 0.107	0.550 ± 0.188	0.690 ± 0.104	0.603 ± 0.095	<b>0.066 ± 0.024</b>
tDCS FOG	A1	Multi-site Transfer	DeFOG + Daphnet	0.513 ± 0.007	0.539 ± 0.147	0.649 ± 0.084	0.711 ± 0.095	0.545 ± 0.126	0.365 ± 0.170	0.501 ± 0.080	0.496 ± 0.115	0.085 ± 0.033
		Adversarial debiasing (Single attribute)	-	0.722 ± 0.019	0.614 ± 0.081	0.598 ± 0.064	0.591 ± 0.060	0.660 ± 0.060	0.543 ± 0.083	0.658 ± 0.054	0.624 ± 0.053	0.228 ± 0.040
		Adversarial debiasing (Multi-Head MLP)	-	0.718 ± 0.013	0.654 ± 0.091	0.644 ± 0.077	0.605 ± 0.064	0.775 ± 0.055 <sup>*</sup>	0.597 ± 0.097	0.665 ± 0.056	0.594 ± 0.053	0.118 ± 0.033
	A2	Multi-site Transfer	DeFOG + Daphnet	0.710 ± 0.024	0.515 ± 0.073	0.590 ± 0.061	0.534 ± 0.060	0.671 ± 0.057	0.452 ± 0.073	0.622 ± 0.047	0.561 ± 0.055	0.203 ± 0.038
		Adversarial debiasing (Single attribute)	-	0.752 ± 0.022 <sup>*</sup>	0.658 ± 0.078	0.578 ± 0.054	0.626 ± 0.056	0.747 ± 0.043 <sup>*</sup>	0.636 ± 0.072 <sup>*</sup>	0.704 ± 0.055	0.680 ± 0.044 <sup>*</sup>	0.214 ± 0.038
		Adversarial debiasing (Multi-Head MLP)	-	0.717 ± 0.021	0.627 ± 0.065	0.576 ± 0.048	0.602 ± 0.050	0.739 ± 0.063	0.536 ± 0.070	0.635 ± 0.046	0.614 ± 0.055	0.142 ± 0.034
	A3	Multi-site Transfer	DeFOG + Daphnet	<b>0.762 ± 0.020</b>	<b>0.654 ± 0.071</b>	0.571 ± 0.061	0.611 ± 0.056	0.706 ± 0.057	0.599 ± 0.078	<b>0.718 ± 0.050</b>	0.647 ± 0.051	0.243 ± 0.047
		×	-	0.724 ± 0.025	0.326 ± 0.080	0.340 ± 0.076	0.315 ± 0.072	0.488 ± 0.125	0.219 ± 0.069	0.224 ± 0.061	0.217 ± 0.075	0.315 ± 0.083
		Threshold optimizer	-	0.705 ± 0.025	0.296 ± 0.078	0.345 ± 0.080	0.311 ± 0.086	0.508 ± 0.132	0.264 ± 0.062	0.319 ± 0.070	0.317 ± 0.073	0.315 ± 0.083
De Souza	A1	Multi-site Transfer	Daphnet	0.724 ± 0.025	0.326 ± 0.080	0.340 ± 0.076	0.315 ± 0.072	0.488 ± 0.125	0.219 ± 0.069	0.224 ± 0.061	0.217 ± 0.075	0.315 ± 0.083
		×	-	<b>0.778 ± 0.033</b>	<b>0.464 ± 0.080</b>	0.423 ± 0.078	<b>0.481 ± 0.082</b>	<b>0.786 ± 0.078</b>	0.317 ± 0.060	0.362 ± 0.073	0.404 ± 0.075	<b>0.191 ± 0.070</b>
		Adversarial debiasing (Single attribute)	-	0.777 ± 0.022	0.455 ± 0.082	0.446 ± 0.080	0.472 ± 0.084	0.541 ± 0.112	0.328 ± 0.074	<b>0.391 ± 0.086</b>	<b>0.416 ± 0.082</b>	0.308 ± 0.082
	A2	Adversarial debiasing (Multi-Head MLP)	-	0.785 ± 0.027	0.411 ± 0.055	<b>0.460 ± 0.057</b>	0.467 ± 0.059	0.653 ± 0.078	0.315 ± 0.046	0.409 ± 0.063	0.376 ± 0.053	0.258 ± 0.059
		Multi-site Transfer	Daphnet	0.774 ± 0.034	0.458 ± 0.083	0.399 ± 0.074	0.438 ± 0.074	0.757 ± 0.101	<b>0.369 ± 0.072</b>	0.283 ± 0.058	0.356 ± 0.065	0.208 ± 0.087
		Adversarial debiasing (Single attribute)	-	0.768 ± 0.017	0.392 ± 0.086	0.387 ± 0.065	0.439 ± 0.057	0.610 ± 0.113	0.316 ± 0.079	0.353 ± 0.075	0.320 ± 0.053	0.276 ± 0.084
	A3	Adversarial debiasing (Multi-Head MLP)	-	0.770 ± 0.038	0.412 ± 0.089	0.417 ± 0.081 <sup>*</sup>	0.444 ± 0.091	0.584 ± 0.084	0.300 ± 0.076	0.347 ± 0.089	0.308 ± 0.068	0.320 ± 0.069
		Multi-site Transfer	Daphnet	0.758 ± 0.036	0.387 ± 0.087	0.376 ± 0.071	0.448 ± 0.080	0.769 ± 0.076	0.287 ± 0.077	0.253 ± 0.065	0.317 ± 0.070	0.213 ± 0.076
		×	-	0.560 ± 0.026	0.370 ± 0.244	0.341 ± 0.181	0.405 ± 0.181	0.668 ± 0.102	0.126 ± 0.154	0.139 ± 0.136	0.203 ± 0.149	0.124 ± 0.042
Daphnet	A1	Threshold optimizer	-	0.533 ± 0.010	0.109 ± 0.060	0.101 ± 0.113	0.023 ± 0.013	0.129 ± 0.086	0.190 ± 0.130	0.112 ± 0.083	0.252 ± 0.108	0.214 ± 0.114
		Multi-site Transfer	De Souza	0.523 ± 0.014	<b>0.655 ± 0.194</b>	0.303 ± 0.464	0.536 ± 0.283	0.032 ± 0.063	0.207 ± 0.278	0.293 ± 0.444	0.207 ± 0.278	0.214 ± 0.114
		×	-	0.613 ± 0.037	0.330 ± 0.114	0.383 ± 0.101	0.401 ± 0.105	0.245 ± 0.138	0.185 ± 0.090	0.312 ± 0.107	0.285 ± 0.108	0.303 ± 0.094
	A2	Adversarial debiasing (Single Attribute)	-	0.602 ± 0.022	0.378 ± 0.165	0.368 ± 0.101	0.377 ± 0.131	0.180 ± 0.158	0.223 ± 0.137	0.306 ± 0.123	0.241 ± 0.155	0.317 ± 0.104
		Adversarial debiasing (Multi-MLP Head)	-	0.649 ± 0.025	0.334 ± 0.115	0.407 ± 0.115	0.442 ± 0.118	0.337 ± 0.109	0.194 ± 0.091	0.383 ± 0.114	0.284 ± 0.107	0.332 ± 0.059
		Multi-site Transfer	De Souza	0.651 ± 0.023	0.301 ± 0.124	0.579 ± 0.106 <sup>*</sup>	0.425 ± 0.116	0.316 ± 0.147	0.177 ± 0.105	0.409 ± 0.099	0.268 ± 0.109	0.337 ± 0.089
	A3	Adversarial debiasing (Single Attribute)	-	0.586 ± 0.013	0.260 ± 0.139	0.473 ± 0.165	0.460 ± 0.155	<b>0.439 ± 0.149</b>	0.129 ± 0.086	0.281 ± 0.144	0.224 ± 0.127	<b>0.187 ± 0.070</b>
		Adversarial debiasing (Multi-MLP Head)	-	0.578 ± 0.024	0.350 ± 0.152	0.417 ± 0.143	0.405 ± 0.140	0.385 ± 0.120	0.137 ± 0.093	0.256 ± 0.123	0.211 ± 0.111	0.214 ± 0.057
		Multi-site Transfer	De Souza	<b>0.667 ± 0.026</b>	0.409 ± 0.143	<b>0.581 ± 0.089</b>	<b>0.499 ± 0.128</b>	0.317 ± 0.138 <sup>*</sup>	<b>0.285 ± 0.138</b>	0.486 ± 0.093 <sup>*</sup>	0.346 ± 0.131 <sup>*</sup>	0.378 ± 0.081

**TABLE 5** Model performance and fairness of the finetuned large pretrained models (foundation models) on the FOG detection task in comparison to the baseline model (A2). **Bold** text indicates the best value in each column for each dataset. \* indicates a statistically significant improvement ( $p \leq 0.05$ , Wilcoxon Signed Rank test (Woolson, 2007)) comparing each bias mitigation method to the baseline ( $\times$  in Bias mitigation column) within the same dataset. Generic activity feature transfer uses a model pretrained on the unlabeled UK Biobank dataset (Doherty et al., 2017) and finetuned on the target dataset (in the Dataset column). Foundation model feature transfer uses a model pretrained on accelerometer data from NHANES dataset (Centers for Disease Control and Prevention and others, 2019; Ruan et al., 2025) and finetuned on the target dataset in the Dataset column.

Dataset	Model	Bias mitigation	F1-score	Demographic Parity Ratio (DPR)				Equalized Odds Ratio (EOR)				Equality of Opportunity Difference (EOD)
				Sex	Age	Disease duration	FOG phenotype	Sex	Age	Disease duration	FOG phenotype	
DeFOG	A2	$\times$	0.582 $\pm$ 0.010	0.402 $\pm$ 0.068	0.528 $\pm$ 0.076	0.569 $\pm$ 0.077	0.418 $\pm$ 0.064	0.300 $\pm$ 0.054	0.320 $\pm$ 0.058	0.382 $\pm$ 0.064	0.183 $\pm$ 0.027	
	B1	Generic Activity Feature Transfer	<b>0.659 <math>\pm</math> 0.012</b>	0.522 $\pm$ 0.068	0.539 $\pm$ 0.063	0.592 $\pm$ 0.073	0.530 $\pm$ 0.060	0.366 $\pm$ 0.058	0.395 $\pm$ 0.065	0.475 $\pm$ 0.071	0.225 $\pm$ 0.033	
	B2	Foundation Model Feature Transfer	0.592 $\pm$ 0.010	<b>0.639 <math>\pm</math> 0.080*</b>	<b>0.657 <math>\pm</math> 0.097*</b>	<b>0.621 <math>\pm</math> 0.088*</b>	<b>0.853 <math>\pm</math> 0.099*</b>	<b>0.501 <math>\pm</math> 0.083*</b>	<b>0.553 <math>\pm</math> 0.093*</b>	<b>0.509 <math>\pm</math> 0.087*</b>	<b>0.111 <math>\pm</math> 0.106</b>	
tDCS FOG	A2	$\times$	0.722 $\pm$ 0.019	0.614 $\pm$ 0.081	0.598 $\pm$ 0.064	0.591 $\pm$ 0.060	0.660 $\pm$ 0.060	0.543 $\pm$ 0.083	0.658 $\pm$ 0.054	0.624 $\pm$ 0.053	0.228 $\pm$ 0.040	
	B1	Generic Activity Feature Transfer	<b>0.763 <math>\pm</math> 0.024</b>	0.584 $\pm$ 0.086	0.567 $\pm$ 0.074	0.573 $\pm$ 0.074	0.572 $\pm$ 0.069	0.523 $\pm$ 0.088	0.615 $\pm$ 0.060	0.563 $\pm$ 0.057	0.321 $\pm$ 0.055	
	B2	Foundation Model Feature Transfer	0.558 $\pm$ 0.020	<b>0.855 <math>\pm</math> 0.060*</b>	<b>0.820 <math>\pm</math> 0.049*</b>	<b>0.850 <math>\pm</math> 0.038*</b>	<b>0.939 <math>\pm</math> 0.025*</b>	<b>0.805 <math>\pm</math> 0.053*</b>	<b>0.834 <math>\pm</math> 0.050*</b>	<b>0.863 <math>\pm</math> 0.052*</b>	<b>0.099 <math>\pm</math> 0.027</b>	
De Souza	A2	$\times$	<b>0.778 <math>\pm</math> 0.033</b>	0.464 $\pm$ 0.080	0.423 $\pm$ 0.078	0.481 $\pm$ 0.082	<b>0.786 <math>\pm</math> 0.078</b>	0.317 $\pm$ 0.060	0.362 $\pm$ 0.073	0.404 $\pm$ 0.075	<b>0.191 <math>\pm</math> 0.070</b>	
	B1	Generic Activity Feature Transfer	0.721 $\pm$ 0.026	0.422 $\pm$ 0.079	0.511 $\pm$ 0.076	0.491 $\pm$ 0.070	0.720 $\pm$ 0.111	0.358 $\pm$ 0.068	0.347 $\pm$ 0.075	0.381 $\pm$ 0.068	0.213 $\pm$ 0.082	
	B2	Foundation Model Feature Transfer	0.666 $\pm$ 0.032	<b>0.471 <math>\pm</math> 0.079</b>	<b>0.605 <math>\pm</math> 0.079*</b>	<b>0.624 <math>\pm</math> 0.072*</b>	0.584 $\pm$ 0.113	<b>0.366 <math>\pm</math> 0.072</b>	<b>0.405 <math>\pm</math> 0.072</b>	<b>0.467 <math>\pm</math> 0.078</b>	0.391 $\pm$ 0.081	
Daphnet	A2	$\times$	<b>0.644 <math>\pm</math> 0.031</b>	0.273 $\pm$ 0.102	0.392 $\pm$ 0.095	0.345 $\pm$ 0.093	0.245 $\pm$ 0.138	0.132 $\pm$ 0.072	0.323 $\pm$ 0.102	0.224 $\pm$ 0.097	0.303 $\pm$ 0.094	
	B1	Generic Activity Feature Transfer	0.644 $\pm$ 0.032	<b>0.449 <math>\pm</math> 0.160</b>	0.411 $\pm$ 0.116	0.439 $\pm$ 0.116	0.293 $\pm$ 0.125	0.132 $\pm$ 0.083	0.208 $\pm$ 0.080	0.167 $\pm$ 0.068	0.267 $\pm$ 0.053	
	B2	Foundation Model Feature Transfer	0.615 $\pm$ 0.022	0.412 $\pm$ 0.095*	<b>0.529 <math>\pm</math> 0.098*</b>	<b>0.512 <math>\pm</math> 0.082*</b>	0.425 $\pm$ 0.111*	0.202 $\pm$ 0.078*	0.371 $\pm$ 0.085*	0.286 $\pm$ 0.081*	<b>0.263 <math>\pm</math> 0.052</b>	

**TABLE 6** Summary of the average performance (F1-score) and fairness (DPR, EOR, and EOD) across multi-site datasets before applying any bias mitigation approaches.

Model	F1-score	DPR FOG phenotype	EOD FOG phenotype	DPR Sex	DPR Age	DPR Disease duration	EOR Sex	EOR Age	EOR Disease duration
A1	0.578	0.435	0.119	0.413	0.467	0.429	0.243	0.292	0.287
A2	0.682	0.527	0.226	0.438	0.486	0.500	0.323	0.416	0.408
A3	0.688	0.540	0.233	0.514	0.463	0.509	0.374	0.403	0.374

**TABLE 7** Description of the FOG-provoking tasks, location of study, medication states for the four multi-site datasets used.

Dataset	Location	Medication States	Study Protocol
DeFOG	Home	On and off	<p>Four meter walk test</p> <p>Timed Up &amp; Go (TUG): series of tasks including rising from a chair, walking a distance of 3 meters, walking back to a chair and sitting down (Podsiadlo and Richardson, 1991).</p> <p>TUG dual task: TUG test with mental subtraction of numbers (Howard et al., 2023).</p> <p>Hotspot Door task: Walking trial involving opening a door, entering another room, and returning to the starting point (Howard et al., 2023).</p> <p>Personalized Hostspot Door task: walking through an area in the house identified as FOG-provoking (Howard et al., 2023).</p>
tDCS FOG	Clinic	On and off	<p>Single task: sit on a chair, rise up &amp; start walking, turn 360 degrees clockwise and counterclockwise, walk 2 meters, open a door, go through, turn 180 degrees, and then go back and sit on the chair (Ziegler et al., 2010).</p> <p>Dual motor task: perform a single task while carrying a tray with a bottle on it (Reches et al., 2020).</p> <p>Motor cognitive task: performing the dual motor task while performing serial seven subtractions (Reches et al., 2020).</p>
Daphnet	Clinic	On and off	Daily walking tasks: walking back and forth in a straight line with random 180-degree turns, random walking with a series of initiated stops and 360-degree turns.
De Souza	Clinic	Off	Turning tasks: turning in place, alternating 360-degree turns to the right and then to the left, and repeating turning at a self-selected pace for two minutes.